

**Please cite the Published Version**

Ray, Nicola J, Kanel, Prabesh and Bohnen, Nicolaas I (2023) Atrophy of the cholinergic basal forebrain can detect presynaptic cholinergic loss in Parkinson's Disease. *Annals of Neurology*, 93 (5). pp. 991-998. ISSN 0364-5134

**DOI:** <https://doi.org/10.1002/ana.26596>

**Publisher:** Wiley

**Version:** Published Version

**Downloaded from:** <https://e-space.mmu.ac.uk/632907/>


**Usage rights:**  [Creative Commons: Attribution-Noncommercial 4.0](https://creativecommons.org/licenses/by-nc/4.0/)

**Additional Information:** This is an open access article which originally appeared in *Annals of Neurology*, published by Wiley

**Enquiries:**

If you have questions about this document, contact [rsl@mmu.ac.uk](mailto:rsl@mmu.ac.uk). Please include the URL of the record in e-space. If you believe that your, or a third party's rights have been compromised through this document please see our Take Down policy (available from <https://www.mmu.ac.uk/library/using-the-library/policies-and-guidelines>)

# Atrophy of the Cholinergic Basal Forebrain can Detect Presynaptic Cholinergic Loss in Parkinson's Disease

Nicola J. Ray, PhD <sup>1</sup>, Prabesh Kanel, PhD,<sup>2,3,4</sup> and Nicolaas I. Bohnen, MD, PhD<sup>2,3,4,5,6</sup>

**Objectives:** Structural imaging of the cholinergic basal forebrain may provide a biomarker for cholinergic system integrity that can be used in motor and non-motor outcome studies in Parkinson's disease. However, no prior studies have validated these structural metrics with cholinergic nerve terminal in vivo imaging in Parkinson's disease. Here, we correlate cholinergic basal forebrain morphometry with the topography of vesicular acetylcholine transporter in a large Parkinson's sample.

**Methods:** [<sup>18</sup>F]-Fluoroethoxybenzovesamicol vesicular acetylcholine transporter positron emission tomography was carried out in 101 non-demented people with Parkinson's (76.24% male, mean age 67.6 ± 7.72 years, disease duration 5.7 ± 4.4 years). Subregional cholinergic basal forebrain volumes were measured using magnetic resonance imaging morphometry. Relationships were assessed via volume-of-interest based correlation analysis.

**Results:** Subregional volumes of the cholinergic basal forebrain predicted cholinergic nerve terminal loss, with most robust correlations occurring between the posterior cholinergic basal forebrain and temporofrontal, insula, cingulum, and hippocampal regions, and with modest correlations in parieto-occipital regions. Hippocampal correlations were not limited to the cholinergic basal forebrain subregion Ch1-2. Correlations were also observed in the striatum, thalamus, and brainstem.

**Interpretation:** Cholinergic basal forebrain morphometry is a robust predictor of regional cerebral vesicular acetylcholine transporter bindings, especially in the anterior brain. The relative lack of correlation between parieto-occipital binding and basal forebrain volumes may reflect the presence of more diffuse synaptopathy in the posterior cortex due to etiologies that extend well beyond the cholinergic system.

ANN NEUROL 2023;93:991–998

## Introduction

Cholinergic degeneration is a major feature of Alzheimer's disease (AD) and dementia with Lewy bodies, but each are associated with differential vulnerability of cholinergic projections.<sup>1</sup> There is also significant, but variable, involvement of cholinergic decline in Parkinson's disease (PD), which has been linked with heterogeneity of PD symptoms.<sup>2–5</sup> However, we do not have a clear

understanding of the spatiotemporal patterns of cholinergic basal forebrain (cBF) nuclei degeneration in PD and resulting denervation of projection sites.

Several positron emission tomography (PET) radiotracers have been developed to assess the loss of cholinergic innervation, with <sup>18</sup>F-fluoroethoxybenzovesamicol ([<sup>18</sup>F]-FEOBV) emerging recently. This tracer binds with high affinity and selectivity to the vesicular acetylcholine

View this article online at [wileyonlinelibrary.com](https://onlinelibrary.wiley.com/doi/10.1002/ana.26596). DOI: 10.1002/ana.26596

Received Aug 25, 2022, and in revised form Dec 19, 2022. Accepted for publication Jan 2, 2023.

Address correspondence to Ray, Health, Psychology and Communities Research Centre, Department of Psychology, Manchester Metropolitan University, Manchester, UK. E-mail: [n.ray@mmu.ac.uk](mailto:n.ray@mmu.ac.uk)

From the <sup>1</sup>Health, Psychology and Communities Research Centre, Department of Psychology, Manchester Metropolitan University, Manchester, UK; <sup>2</sup>Radiology, University of Michigan, Ann Arbor, Michigan, USA; <sup>3</sup>Morris K. Udall Center of Excellence for Parkinson's Disease Research, University of Michigan, Ann Arbor, Michigan, USA; <sup>4</sup>Parkinson's Foundation Center of Excellence, University of Michigan, Ann Arbor, Michigan, USA; <sup>5</sup>Neurology, University of Michigan, Ann Arbor, Michigan, USA; and <sup>6</sup>Neurology Service and GRECC, Veterans Administration Ann Arbor Healthcare System, Ann Arbor, Michigan, USA

Additional supporting information can be found in the online version of this article.

transporter (VACHT),<sup>6</sup> a glycoprotein found essentially in cholinergic synapses, and can therefore index presynaptic cholinergic nerve terminal loss. Recent studies indicate that [<sup>18</sup>F]-FEOBV can distinguish controls from people with AD<sup>7</sup> or dementia with Lewy bodies,<sup>8</sup> and is sensitive to cognitive<sup>2, 9</sup> and cardinal motor symptoms,<sup>10</sup> most notably balance and gait deficits.<sup>3</sup>

The main source of cholinergic input to the cerebral cortex is the cBF, which consists of the nucleus basalis Meynert (NBM), the horizontal and diagonal band of Broca, and the nucleus subputaminalis (a distinct cluster lateral to the anterior commissure and ventral to the putamen).<sup>11, 12</sup> In Mesulam's nomenclature, Ch1 corresponds to the medial septal nuclei, Ch2 to the vertical part of the diagonal band of Broca, Ch3 to the horizontal part of the diagonal band of Broca, and Ch4 to the NBM. Ch4 is further divided into the posterior (Ch4p), intermediate (Ch4i), anterior-medial (Ch4am), and anterior-lateral parts (Ch4al). Histological analysis has revealed that Ch1 and Ch2 mainly supply the hippocampus formation, Ch3 the olfactory bulb, while the anterior Ch4 regions project to widespread areas of cortex, and the posterior Ch4 region to superior temporal and midtemporal cortex.<sup>11</sup>

In AD, there is a concordance between the topography of cortical [<sup>18</sup>F]-FEOBV uptake and cBF neurodegeneration as estimated with magnetic resonance imaging (MRI) volumetry.<sup>7</sup> Thus, atrophy of the anterior-intermediate and posterior subregions of Ch4 were correlated with reduced [<sup>18</sup>F]-FEOBV binding in their projection regions: the frontal/cingulate cortex and superior temporal cortex, respectively. On the other hand, there was no correlation between volumetry in the Ch1-2 region, which may not degenerate in early AD stages,<sup>13</sup> and [<sup>18</sup>F]-FEOBV uptake in hippocampal projection sites.

In PD, cBF volumetry has revealed that the region degenerates early and is associated with more rapid progression of cognitive decline.<sup>13-18</sup> However, we do not know how this cBF degeneration is associated with regional loss of functional cholinergic integrity in the wider brain as measured with [<sup>18</sup>F]-FEOBV PET. Revealing the relationships between cBF atrophy and whole-brain cholinergic innervation would enable the characterization of the regional functional implications that accompany structural degeneration in the cBF.

The purpose of the current study, therefore, was to examine the topographic relationship between degeneration in sub-regions of the cBF and regional [<sup>18</sup>F]-FEOBV binding in nondemented people with PD. Since in vivo VACHT binding studies have shown early vulnerability of posterior cortical regions in PD,<sup>19, 20</sup> we expected to

observe strong correlations between posterior cortical VACHT binding and regional volume loss (especially Ch4ai) compared to anterior cortical regions.

## Methods

The protocol for this study received prior approval by the Institutional Review Boards of the University of Michigan and Ann Arbor VA Healthcare and completed in compliance with the Declaration of Helsinki guideline. Informed consent was obtained from each subject prior to their participation.

### Participants

This study involved 112 participants with PD, with 101 having images suitable for analysis (77 males; 24 females), mean age  $67.6 \pm 7.72$  years. All met the UK Parkinson's Disease Society Brain Bank clinical diagnostic criteria.<sup>21</sup> Participants with evidence of large vessel stroke or other intracranial lesions on anatomic imaging were excluded. All participants had PET and T1-weighted images available.

**Clinical Measures.** The Unified Parkinson's Disease Rating scale (UPDRS) Part III and Montreal Cognitive Assessment (MoCA) are used as measures of motor symptom severity and cognitive health, respectively. Participants with MoCA below 26 were defined as having evidence of mild cognitive impairment (MCI).

## Imaging Methods

### Imaging Acquisition

**Positron Emission Tomography.** [<sup>18</sup>F]-FEOBV PET imaging was performed in 3D imaging mode with a Siemens ECAT Exact HR+ tomograph or Biograph 6 TruPoint PET/computed tomography scanner (Siemens Molecular Imaging, Inc., Knoxville, TN), which acquire 63 transaxial slices (slice thickness: 2.4 mm) over a 15.2 cm axial field of view (FOV). Images were corrected for scatter and motion. Subjects were scanned in the dopaminergic medication "on" state. Data harmonization for the two scanners was performed as previously reported.<sup>22</sup>

[<sup>18</sup>F]-FEOBV was prepared as described previously.<sup>23</sup> [<sup>18</sup>F]-FEOBV delayed dynamic imaging was performed over 30 minutes (in six 5 minute frames) starting 3 hours after an intravenous bolus dose injection of 8 mCi [<sup>18</sup>F]-FEOBV. PET imaging frames were spatially coregistered within subjects with a rigid-body transformation to reduce the effects of subject motion during the imaging session.

A white matter (WM) reference tissue approach was used to determine VACHT binding as previously reported.<sup>24</sup> Distribution volume ratios (DVRs) were

calculated from ratio of summed six delayed imaging frames (3 hours after injection) for grey matter (GM) target and WM reference tissues.<sup>25</sup>

**Volumetric T1-Weighted Acquisition.** MRI was performed on a 3 Tesla Philips Achieva system (Philips, Best, The Netherlands). For volumetric T1-weighted images, a three-dimensional (3D) inversion recovery-prepared turbo field echo was performed in the sagittal plane using repetition time/echo time/inversion time = 9.8/4.6/1041 ms; turbo factor = 200; single average; FOV = 240 × 200 × 160 mm; acquired matrix = 240 × 200 × 160 slices; and reconstructed to 1-mm isotropic resolution.

### Image Preprocessing

**PET.** Statistical parametric mapping (SPM) software (SPM12; Wellcome Trust Centre for Neuroimaging, University College, London, England [<https://www.fil.ion.ucl.ac.uk/spm/software/spm12/>]) was used for PET-MRI registration using the cropped T1-weighted MR volumetric scan. Freesurfer software (<http://surfer.nmr.mgh.harvard.edu>) was used to define cortical and subcortical MR gray volumes of interest (VOIs). PET-MRI coregistration was performed as previously reported.<sup>8, 26</sup> Partial volume corrections were performed using the Müller-Gärtner method.<sup>25</sup> The Müller-Gärtner method uses registered GM and WM segmentation to label each PET voxel into GM and WM regions. Using these PET's GM, WM, and resolution, the spill-out from the WM to GM regions is estimated and removed. Similarly, the method estimates GM spill-out to the surrounding areas and compensates. The Müller-Gärtner method produces a GM image with corrected GM values in all voxels.

### T1-Weighted Volumetric Images

T1 scans were automatically segmented into GM, WM, and cerebrospinal fluid (CSF) partitions of 1.5 mm isotropic voxel size using the segmentation routine of the CAT12 toolbox (<https://neuro-jena.github.io/cat/>) running under SPM12 (<http://www.fil.ion.ucl.ac.uk/spm/software/spm12/>). The resulting grey and WM partitions of each subject in native space were then high-dimensionally registered to Montreal Neurological Institute (MNI) space using DARTEL.<sup>27</sup> The GM segments were then warped using the individual flow fields resulting from the DARTEL registration, and voxel values were modulated for volumetric changes introduced by the high-dimensional normalization. Thus, the total amount of GM volume present before warping was preserved. All preprocessed GM maps were required to pass

a visual inspection for overall segmentation and registration accuracy. This resulted in removal of 11 participant's images. We believe poor quality of the raw image, potentially due to movements in our population of participants, is the reason for the excluded images. Extractions of volumetric data from regions of interest (ROIs, see below) were performed in MNI space. Mean volumes were calculated for ROIs across both hemispheres, and normalized via analysis of covariance by total intracranial volume (TIV, calculated as the sum of GM, WM, and CSF).

### Regions of Interest

A map of the cBF was created as described in Kilimann et al.<sup>13</sup> In brief, the map was derived from combined post-mortem MRI and subsequent histological preparation of a brain specimen of a 56-year-old male who had died without any evidence of cognitive decline or psychiatric illnesses. Cerebral MRI scans were performed in situ. Cholinergic nuclei were identified and delineated on digital pictures of the stained brain slices, then manually transferred from the digital pictures into the corresponding MRI slices before final transformation into MNI space using DARTEL. The stereotactic cBF map distinguishes different cholinergic subdivisions, including regions that correspond to medial septum and vertical limb of the diagonal band (Ch1-2 in Mesulam's nomenclature<sup>11</sup>), horizontal limb of the diagonal band (Ch3), anterior and intermediate NBM (Ch4a-i), the anterolateral NBM/nucleus subputaminalis (Ch4a/NSP), and posterior parts of the NbM (Ch4p).

### Statistical Analysis

Statistical analyses were conducted in SPM12 and SPSS 27.

Relationships between [<sup>18</sup>F]-FEOBV in VOIs and sub-regional cBF volumes were assessed with two-tailed bivariate Pearson's correlations, with family-wise error (FWE) correction for multiple comparisons across all cortical and subcortical VOIs. Significant outcomes were further assessed with control for age, and surviving outcomes were further controlled for age and disease duration using partial correlations.

We repeated the analysis above for participants with MCI as defined above. These outcomes were qualitatively compared with those from a similarly sized ( $N = 38$ ) group of participants without any evidence of MCI (ie, with MoCA  $\geq 26$ ). Please note that these results have not been corrected for multiple comparisons as they are presented for comparison with the full dataset only, and not findings in their own right.

**Table. Demographics of 101 Participants with Parkinson's Disease (76.24% = male, 37.6% with MoCA  $\leq$  25)**

	Mean	Standard Deviation	Min	Max
Age (years)	67.6	7.73	50	93
Duration (Months)	5.8	4.39	1	30
MDS-UPDRS-III	34.2	12.51	9	73
Hoehn and Yahr	2.4	0.63	1	4
MoCA	26.1	3.15	10	30

Abbreviations: MDS-UPDRS-III, Part III of the Unified Parkinson's Disease Rating Scale; MoCA, Montreal Cognitive Assessment.

## Results

Brief clinical and demographic characteristics can be seen in Table. There were 38 participants with evidence of MCI according to the MoCA.

Table S1 and Figure reports correlations between sub-regional cBF volumes and [ $^{18}$ F]-FEOBV uptake, with and without control for age and disease duration. In brief, the region corresponding to the posterior NBM was significantly correlated with widespread VOIs in both hemispheres after FWE correction for multiple comparisons, and after further correction for both age and disease duration. Anterior NBM regions showed correlations with VOIs primarily in temporal and hippocampal regions.

For qualitative comparison, Tables S2 and S3 report the same correlations performed separately in the group with/without evidence of cognitive impairment, as defined above.

Volumes in the Ch3 region showed similar relationships to those observed between posterior NBM and [ $^{18}$ F]-FEOBV uptake. In Ch1-2, the strongest correlations were seen for hippocampal, temporal and cingulate regions (FWE corrected statistics are reported in Table S1). All regions of the cBF were correlated with [ $^{18}$ F]-FEOBV in the hippocampus (Table S1 and Figure).

## Discussion

Overall, we found robust correlations between regional cBF morphometry and regional cortical VAcHT binding, except for in the posterior cortices. In general, these outcomes survived control for age and disease duration in a pattern that largely depended on the strength of the zero-order correlations. Prior VAcHT FEOBV brain PET imaging studies have shown evidence of early vulnerability of occipital and parietal cortices in PD.<sup>19, 20</sup> This

observation is consistent with (cross-sectional) findings of a suggested posterior-to-anterior cortical denervation gradient from PD to PD with dementia in VAcHT SPECT and AChE PET studies.<sup>28, 29</sup> In contrast, preserved to even upregulated cholinergic VAcHT binding has been observed in the anterior (frontal, anterior temporal) cortices, amygdala, hippocampus, basal ganglia, thalamus, with relative sparing of the posterior cingulum in a recent [ $^{18}$ F]-FEOBV PET study.<sup>19</sup>

These regional cerebral cholinergic nerve terminal changes seen in in vivo imaging studies suggest that cBF cortical projections of the NBM would primarily correlate with VAcHT losses in parieto-occipital cortices compared to anterior brain regions in the PD population. However, in our analysis, we showed no significant correlations between the anterior regions of the NBM and the cuneus regions or lateral occipital regions, and only weak to modest correlations with the lingual and pericalcarine regions. Correlations were also absent for anterior Ch4 morphometry and the inferior parietal, superior parietal and only weak to modest correlations with the supramarginal parietal cortices.

These observations do not support our a priori hypothesis, and our findings do not appear to support the long-held understanding that longer axonal projections are more vulnerable to degeneration to explain to more prominent posterior cortical cholinergic nerve terminal losses.<sup>30</sup> It is possible that the absence of such relationship may relate to statistical "floor" denervation effects in posterior cortical regions, as has been shown for posterior putaminal presynaptic dopaminergic nerve terminal losses in PD.<sup>31</sup> Indeed, we observed particularly weak relationships between posterior [ $^{18}$ F]-FEOBV uptake and cBF morphometry in a sub-group of participants with evidence of cognitive impairment, who would be expected to have both higher levels of atrophy and more extensive cholinergic terminal loss. It should be noted here that denervation floor effects could occur for the measurement of atrophy with morphometry as well as for cholinergic terminal loss measured with PET.

Similarly, robust correlations were seen for para-, pre-, and post-central cortical VAcHT binding with most of the cBF regions. The correlations between para- and pre-central regions are also observed in the surrounding frontal regions. However, the strong correlation seen for the post-central region is not observed in the surrounding parietal cortical regions, where only modest correlations with cBF regions exist. Given that AChE (and also glucose metabolic fluorodexoglucose [FDG]) is preserved in the pericentral cortex in PD compared to the posterior parietal and occipital cortices,<sup>29, 31, 32</sup> this may suggest that additional, non-cholinergic neurodegenerative processes such as more prominent posterior cortical glucose

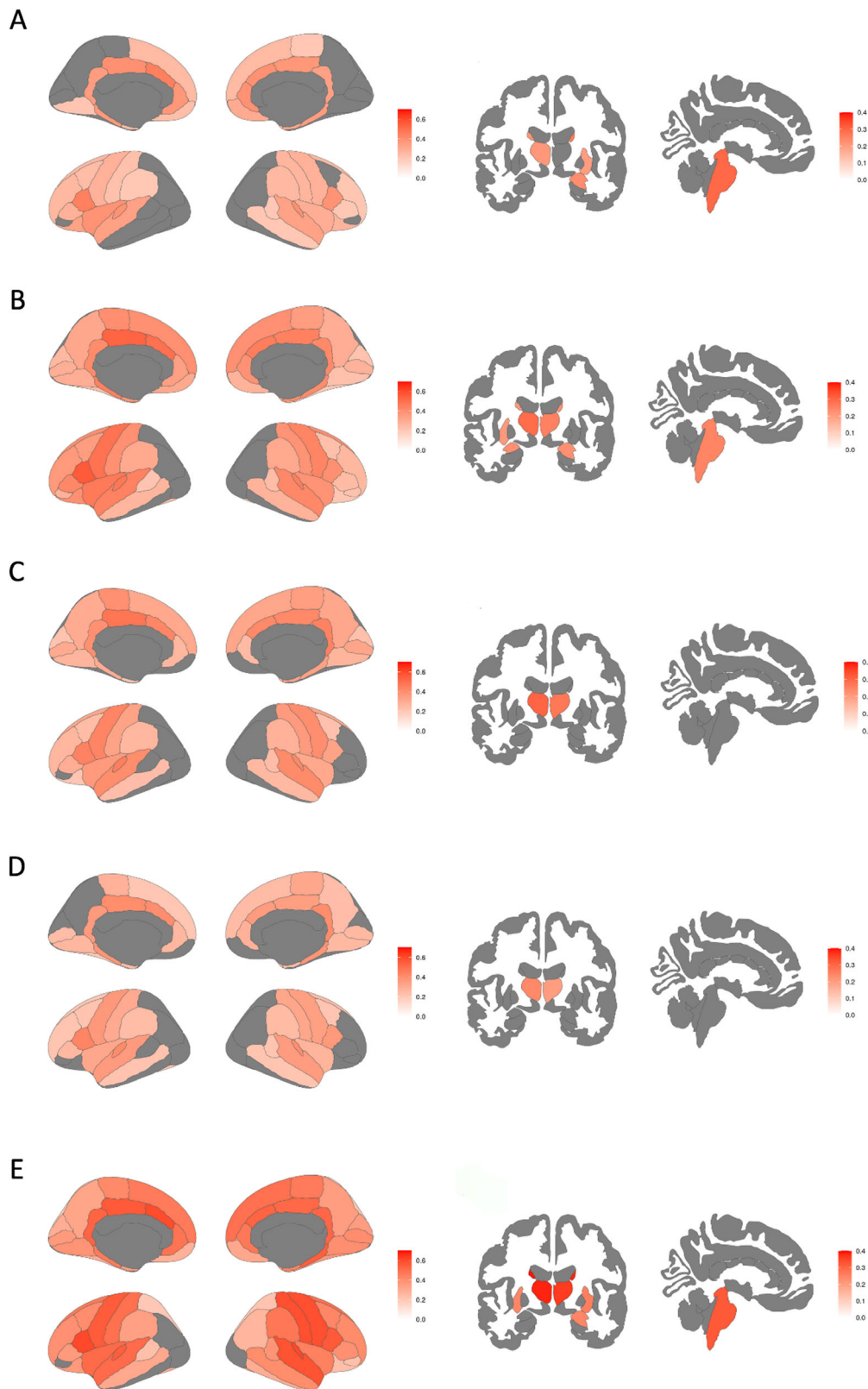


Figure: The Pearson's correlation ( $r$ ) values between [ $^{18}\text{F}$ ]-FEOBV in cortical, subcortical and brainstem volumes of interest and total intracranial volume (TIV)-normalized sub-regional cholinergic basal forebrain volumes. Brain regions in (A) represents significant correlation values between  $^{18}\text{F}$ -fluroethoxybenzovesamicol ([ $^{18}\text{F}$ ]-FEOBV) in cortical, subcortical and brainstem volumes of interest and Ch1-2 volume. Similarly, Brain region in (B), (C), (D), and (E) illustrate the significant Pearson correlation values between [ $^{18}\text{F}$ ]-FEOBV in cortical, subcortical and brainstem volumes of interest and Ch3, Ch4a-i, Ch4a/NSP, and Ch4p respectively. Significant Pearson's  $r$  values are illustrated in white to red color. [Color figure can be viewed at [www.annalsofneurology.org](http://www.annalsofneurology.org)]

hypometabolism and resulting in more diffuse cortical synaptic losses may be obscuring relationships between VAcHT binding in the parieto-occipital cortices and the cBF regions. The relative prominence of correlations between post-central (somatosensory) cortical VAcHT binding and Ch3 and Ch4 may also reflect known anatomic projections.<sup>33</sup>

We observed highly robust correlations between posterior NBM volumes and transverse, middle and superior temporal gyri, and temporal pole regions bilaterally. These findings are unlikely to be explained by concomitant cBF atrophy and lateral temporal cholinergic denervation because previous data suggests there is preserved to upregulated VAcHT binding in the mid to upper temporal cortical regions in PD observed with VAcHT [<sup>18</sup>F]-FEOBV PET.<sup>19</sup> It is possible that preserved to upregulated lateral temporal cholinergic transporter may potentially correspond to upregulated choline acetyltransferase enzyme activity, as has been shown in a post-mortem study of MCI in older adults.<sup>34</sup> Yet, robust correlations were seen with all studied cBF subregions (Ch4p, Ch4a-I, Ch4al NSP, Ch1-2, and Ch3) and cholinergic transporter binding in the transverse temporal and superior (including Wernicke's area, Brodmann area 22) temporal, but not in the inferior temporal gyri. These findings suggest that the mid to upper lateral temporal neocortex may receive wide input from across the different cBF regions. Relatedly, VAcHT binding in most of the prefrontal cortex—including Broca's area (Brodmann areas 44: parts opercularis and 45: pars triangularis) showed robust correlations with all study cBF regions. These correlations may reflect either multi-functional connectivities between these anterior cortical regions and different cBF nuclei or a biological reserve capacity for innervating key cholinergic brain regions. The implication of the latter might indicate therefore that preserved cBF structure, rather than cBF atrophy, underpins both the cBF-temporal and cBF-prefrontal correlations just described.

We also saw strong correlations across cBF subregions and VAcHT binding in the hippocampus, parahippocampal, entorhinal and cingulate cortices, and insula. This may reflect that limbic and paralimbic cortices of the brain receive the heaviest cholinergic input from Ch4 and are also the principal sources of reciprocal cortical projections back to the nucleus basalis.<sup>35</sup> Unlike the hippocampus, few correlations were seen with the amygdala, but this was not with the anterior regions of the cBF as anatomically predicted. This may reflect different (at least in terms of cholinergic neurotransmission) neural circuitry connectivity of the amygdala compared to the hippocampal regions.

Our previous *in vivo* VAcHT [<sup>18</sup>F]-FEOBV bio-distribution study shows several cortical areas (the caudal

anterior cingulum [Brodmann area 24]) and the pericentral cortices (Brodmann areas 1–5) with higher binding intensities compared to the remainder of the cortex.<sup>36</sup> However, all regions in the cingulate cortex demonstrated robust correlations with the cBF region, suggesting that relative VAcHT binding intensities are not influencing the cBF-cingulate correlations observed.

Significant correlations were also seen for the VAcHT binding in striatal (both putamen and caudate) nucleus and the cBF. This may reflect the presence of a subset of Ch1-Ch4 projections to the striatum.<sup>35</sup> Robust correlations were also seen between thalamic VAcHT binding and Ch4p, Ch4ai and Ch3. While most of the thalamic cholinergic input comes from the upper brainstem (Ch5 and Ch6), the intralaminar and reticular nuclei, and especially medially situated patches within the mediodorsal nucleus also appear to receive substantial cholinergic innervation from the cBF.<sup>37</sup> Moderately robust correlations were seen between brainstem VAcHT binding and Ch4 and Ch1-2. This may reflect known connections between the substantial innominate and the lateral preoptic area.<sup>38</sup> No significant correlations were seen between the cBF and the pallidum and nucleus accumbens.

Post-mortem data have shown evidence of Ch4al connections to the amygdala, frontoparietal, and opercular regions.<sup>39</sup> We observed robust correlations between Ch4al/NSP and VAcHT binding in the pars opercularis but not in other frontal or parietal regions. However, robust correlations were seen with VAcHT binding in the cingulate cortex, insula, transverse temporal gyrus, hippocampus, parahippocampal gyri, and pericentral regions.

In AD, atrophy of the Ch4a-I and posterior subregions of Ch4 were correlated with reduced [<sup>18</sup>F]-FEOBV binding in their projection regions: the frontal/cingulate cortex and superior temporal cortex, respectively. However, there was no correlation between volumetry in the Ch1-2 region and VAcHT binding in hippocampus. These findings differ from our present findings in a (non-demented) PD population. While this could reflect intrinsic differences in AD versus PD pathology in the cBF, the differences in sample sizes between the current study and the previous AD study preclude any direct comparisons.

A limitation of this study is that unlike post-mortem tracings studies, assumptions about cBF projections and connectivities are solely based on correlations for which causality cannot be inferred. In addition, there will be a high degree of correlation between volumes that are spatially close together, as in the cBF. It is not possible to control for this shared variance without also removing the

variability in atrophy that we are interested in, and as such, there is likely to be more specificity between cholinergic synaptic terminal loss and sub-regional cBF atrophy than we have reported here. Despite these limitations, our findings show relative specificity of selective cBF and regional brain VAcHT binding.

In summary, given that we did not see evidence of expected correlations between cBF atrophy and known vulnerability of parieto-occipital cholinergic nerve terminals, we conclude that the correlations between regional cBF atrophy measures and topography of nerve terminal losses reported here appear to be driven more by neural circuit or VAcHT regulatory function than vulnerability of long cholinergic axonal projections. This conclusion is consistent with our recently published work showing proportional relationships between posterior cortical acetylcholinesterase activity (measured with [<sup>11</sup>C]-methyl-4-piperidinypropionate) and changes in regional cerebral blood flow, while in frontal regions there was proportionally greater loss of acetylcholinesterase activity relative to changes in blood flow.<sup>40</sup> Together with the current paper, this might indicate that posterior cortical cholinergic synapse deficits reflect a more generalized loss of synapses that do not fully associate with cBF atrophy. On the other hand, there may be a preferential loss or dysregulation of cholinergic synapses in frontal cortical regions that more closely reflects atrophy in the nuclei where these neurons originate.

## Acknowledgments

The authors thank Christine Minderovic, Virginia Rogers, the PET technologists, cyclotron operators, and chemists, for their assistance. This work was supported by the Department of Veterans Affairs grant I01 RX003397, the Michael J. Fox Foundation, Farmer Family Foundation grant, the Parkinson's Foundation, and NIH grants P01 NS015655, RO1 NS070856, P50 NS091856, P50 NS123067, and R01 AG073100.

## Author Contributions

Nicolaas I. Bohnen and Nicola J. Ray contributed to the conception and design of the study; Nicolaas I. Bohnen and Prabesh Kanel contributed to the acquisition and analysis of data; Nicolaas I. Bohnen and Nicola J. Ray contributed to drafting the text and preparing the figures.

## Potential Conflicts of Interest

The authors declare no conflict of interest relevant to this work.

## References

- Kanel P, Bedard MA, Aghourian M, et al. Molecular imaging of the cholinergic system in Alzheimer and Lewy body dementias: expanding views. *Curr Neurol Neurosci Rep* 2021;21:52.
- van der Zee S, Müller M, Kanel P, et al. Cholinergic denervation patterns across cognitive domains in Parkinson's disease. *Mov Disord* 2021;36:642–650.
- Bohnen NI, Kanel P, Zhou Z, et al. Cholinergic system changes of falls and freezing of gait in Parkinson's disease. *Ann Neurol* 2019;85: 538–549.
- Muller ML, Bohnen NI, Kotagal V, et al. Clinical markers for identifying cholinergic deficits in Parkinson's disease. *Mov Disord* 2015;30: 269–273.
- Bohnen NI, Muller ML, Kotagal V, et al. Heterogeneity of cholinergic denervation in Parkinson's disease without dementia. *J Cereb Blood Flow Metab* 2012;32:1609–1617.
- Mulholland GK, Wieland DM, Kilbourn MR, et al. [<sup>18</sup>F] fluoroethoxybenzovesamicol, a PET radiotracer for the vesicular acetylcholine transporter and cholinergic synapses. *Synapse* 1998;30:263–274.
- Aghourian M, Aumont É, Grothe MJ, et al. FEOBV-PET to quantify cortical cholinergic denervation in AD: relationship to basal forebrain volumetry. *J Neuroimaging* 2021;31:1077–1081.
- Kanel P, Müller M, van der Zee S, et al. Topography of cholinergic changes in dementia with Lewy bodies and key neural network hubs. *J Neuropsychiatry Clin Neurosci* 2020;32:370–375.
- Legault-Denis C, Aghourian M, Soucy JP, et al. Normal cognition in Parkinson's disease may involve hippocampal cholinergic compensation: an exploratory PET imaging study with [(18) F]-FEOBV. *Parkinsonism Relat Disord* 2021;91:162–166.
- Bohnen NI, Kanel P, Koeppe RA, et al. Regional cerebral cholinergic nerve terminal integrity and cardinal motor features in Parkinson's disease. *Brain Commun* 2021;3:fcab109.
- Mesulam MM, Mufson EJ, Wainer BH, Levey AI. Central cholinergic pathways in the rat: an overview based on an alternative nomenclature (Ch1-Ch6). *Neuroscience* 1983;10:1185–1201.
- Ayala G. A hitherto undifferentiated nucleus in the forebrain (nucleus subputaminalis). *Brain* 1915;37:433–448.
- Kilimann I, Grothe M, Heinsen H, et al. Subregional basal forebrain atrophy in Alzheimer's disease: a multicenter study. *J Alzheimers Dis* 2014;40:687–700.
- Perry EK, Curtis M, Dick DJ, et al. Cholinergic correlates of cognitive impairment in Parkinson's disease: comparisons with Alzheimer's disease. *J Neurol Neurosurg Psychiatry* 1985;48:413–421.
- Ray NJ, Bradburn S, Murgatroyd C, et al. In vivo cholinergic basal forebrain atrophy predicts cognitive decline in de novo Parkinson's disease. *Brain* 2018;141:165–176.
- Grothe MJ, Labrador-Espinosa MA, Jesús S, et al. In vivo cholinergic basal forebrain degeneration and cognition in Parkinson's disease: imaging results from the COPPADIS study. *Parkinsonism Relat Disord* 2021;88:68–75.
- Pereira JB, Hall S, Jalakas M, et al. Longitudinal degeneration of the basal forebrain predicts subsequent dementia in Parkinson's disease. *Neurobiol Dis* 2020;139:104831.
- Schulz J, Pagano G, Fernandez Bonfante JA, et al. Nucleus basalis of Meynert degeneration precedes and predicts cognitive impairment in Parkinson's disease. *Brain* 2018;141:1501–1516.
- van der Zee S, Kanel P, Gerritsen MJ, et al. Altered cholinergic innervation in De novo Parkinson's disease with and without cognitive impairment. *Mov Disord* 2022;37:713–723.
- van der Zee S, Vázquez García D, Elsinga PH, et al. [<sup>18</sup>F] Fluoroethoxybenzovesamicol in Parkinson's disease patients: quantification of a novel cholinergic positron emission tomography tracer. *Mov Disord* 2019;34:924–926.



21. Hughes AJ, Daniel SE, Kilford L, Lees AJ. Accuracy of clinical diagnosis of idiopathic Parkinson's disease: a clinico-pathological study of 100 cases. *J Neurol Neurosurg Psychiatry* 1992;55:181–184.
22. Kanel P, van der Zee S, Sanchez-Catasus CA, et al. Cerebral topography of vesicular cholinergic transporter changes in neurologically intact adults: a [(18)F]FEOBV PET study. *Aging. Brain* 2022;2:100039.
23. Shao X, Hoareau R, Hockley BG, et al. Highlighting the versatility of the Tracerlab synthesis modules. Part 1: fully automated production of [F]labelled radiopharmaceuticals using a Tracerlab FX(FN). *J Label Compd Radiopharm* 2011;54:292–307.
24. Nejad-Davarani S, Koeppe RA, Albin RL, et al. Quantification of brain cholinergic denervation in dementia with Lewy bodies using PET imaging with [(18)F]-FEOBV. *Mol Psychiatry* 2019;24:322–327.
25. Muller-Gärtner HW, Links JM, Prince JL, et al. Measurement of radio-tracer concentration in brain gray matter using positron emission tomography: MRI-based correction for partial volume effects. *J Cereb Blood Flow Metab* 1992;12:571–583.
26. Bohnen NI, Kanel P, Koeppe RA, et al. Regional cerebral cholinergic nerve terminal integrity and cardinal motor features in Parkinson's disease. *Brain. Communications* 2021;3:fcab109.
27. Ashburner J. A fast diffeomorphic image registration algorithm. *Neuroimage* 2007;38:95–113.
28. Kuhl DE, Koeppe RA, Minoshima S, et al. In vivo mapping of cerebral acetylcholinesterase activity in aging and Alzheimer's disease. *Neurology* 1999;52:691–699.
29. Klein JC, Eggers C, Kalbe E, et al. Neurotransmitter changes in dementia with Lewy bodies and Parkinson disease dementia in vivo. *Neurology* 2010;74:885–892.
30. Mattson MP, Magnus T. Ageing and neuronal vulnerability. *Nat Rev Neurosci* 2006;7:278–294.
31. Bohnen NI, Albin RL, Koeppe RA, et al. Positron emission tomography of monoaminergic vesicular binding in aging and Parkinson disease. *J Cereb Blood Flow Metab* 2006;26:1198–1212.
32. Bohnen NI, Koeppe RA, Minoshima S, et al. Cerebral glucose metabolic features of Parkinson disease and incident dementia: longitudinal study. *J Nucl Med* 2011;52:848–855.
33. Chaves-Coira I, Martín-Cortecero J, Nuñez A, Rodrigo-Angulo ML. Basal forebrain nuclei display distinct projecting pathways and functional circuits to sensory primary and prefrontal cortices in the rat. *Front Neuroanat* 2018;12:69.
34. DeKosky ST, Ikonomic MD, Styren SD, et al. Upregulation of choline acetyltransferase activity in hippocampus and frontal cortex of elderly subjects with mild cognitive impairment. *Ann Neurol* 2002; 51:145–155.
35. Mesulam MM. Cholinergic circuitry of the human nucleus basalis and its fate in Alzheimer's disease. *J Comp Neurol* 2013;521:4124–4144.
36. Albin RL, Bohnen NI, Muller M, et al. Regional vesicular acetylcholine transporter distribution in human brain: a [(18) F] fluoroethoxybenzovesamicol positron emission tomography study. *J Comp Neurol* 2018;526:2884–2897.
37. Heckers S, Geula C, Mesulam MM. Cholinergic innervation of the human thalamus: dual origin and differential nuclear distribution. *J Comp Neurol* 1992;325:68–82.
38. Swanson LW, Mogenson GJ, Gerfen CR, Robinson P. Evidence for a projection from the lateral preoptic area and substantia innominata to the 'mesencephalic locomotor region' in the rat. *Brain Res* 1984; 295:161–178.
39. Liu AK, Chang RC, Pearce RK, Gentleman SM. Nucleus basalis of Meynert revisited: anatomy, history and differential involvement in Alzheimer's and Parkinson's disease. *Acta Neuropathol* 2015;129: 527–540.
40. Bohnen NI, Roytman S, Kanel P, et al. Progression of regional cortical cholinergic denervation in Parkinson's disease. *Brain Comm* 2022.